Acta Oceanol. Sin., 2020, Vol. 39, No. 7, P. 11–18
https://doi.org/10.1007/s13131-020-1576-2
http://www.hyxb.org.cn
E-mail: hyxbe@263.net

Intraseasonal modulation of Wyrtki jet in the eastern Indian Ocean by equatorial waves during spring 2013

Yongliang Duan[1, 2], Hongwei Liu[3, 4, 5], Lin Liu[1, 2*], Weidong Yu[6, 7, 8]

[1] Center for Ocean and Climate Research, First Institute of Oceanography, Ministry of Natural Resources, Qingdao 266061, China

[2] Laboratory for Regional Oceanography and Numerical Modeling, Pilot National Laboratory for Marine Science and Technology (Qingdao), Qingdao 266061, China

[3] Key Laboratory of Ocean Circulation and Waves, Institute of Oceanology, Chinese Academy of Sciences, Qingdao 266071, China

[4] Laboratory for Ocean and Climate Dynamics, Pilot National Laboratory for Marine Science and Technology (Qingdao), Qingdao 266071, China

[5] Center for Ocean Mega-Science, Chinese Academy of Sciences, Qingdao 266071, China

[6] School of Atmospheric Sciences, Sun Yat-Sen University, Zhuhai Campus, Zhuhai 519082, China

[7] Key Laboratory of Tropical Atmosphere-Ocean System (Sun Yat-Sen University), Ministry of Education, Zhuhai 519082, China

[8] Southern Marine Science and Engineering Guangdong Laboratory (Zhuhai), Zhuhai 519082, China

Received 8 January 2020; accepted 4 February 2020

Abstract

A strong spring Wyrtki jet (WJ) presents in May 2013 in the eastern equatorial Indian Ocean. The entire buildup and retreat processes of the spring WJ were well captured by two adjacent Acoustic Doppler Current Profilers mounted on the mooring systems. The observed zonal jet behaved as one intraseasonal event with the significant features of abrupt emergence as well as slow disappearance. Further research illustrate that the pronounced surface westerly wind burst during late-April to mid-May, associated with the active phase of a robust eastward-propagating Madden–Julian oscillation in the tropical Indian Ocean, was the dominant reason for the rapid acceleration of surface WJ. In contrasting, the governing mechanism for the jet termination was equatorial wave dynamics rather than wind forcing. The decomposition analysis of equatorial waves and the corresponding changes in the ocean thermocline demonstrated that strong WJ was produced rapidly by the wind-generated oceanic downwelling equatorial Kelvin wave and was terminated subsequently by the westward-propagating equatorial Rossby wave reflecting from eastern boundaries of the Indian Ocean.

Key words: Wyrtki jet, equatorial wave dynamics, Madden–Julian oscillation, tropical Indian Ocean

Citation: Duan Yongliang, Liu Hongwei, Liu Lin, Yu Weidong. 2020. Intraseasonal modulation of Wyrtki jet in the eastern Indian Ocean by equatorial waves during spring 2013. Acta Oceanologica Sinica, 39(7): 11–18, doi: 10.1007/s13131-020-1576-2

1 Introduction

The surface circulation of the tropical Indian Ocean (TIO) is primary modulated by the seasonal monsoon winds (Schott and McCreary, 2001; Schott et al., 2009). During monsoon transition seasons, the strong eastward surface Wyrtki jets (WJs), forced directly by the semiannual westerly equatorial winds, take place at boreal spring and fall seasons (Wyrtki, 1973; O'Brien and Hurlburt, 1974; Han et al., 1999; McPhaden et al., 2015; Liu et al., 2016). Previous studies on the WJ dynamics, mostly based on the theoretical and linear/nonlinear numerical models (e.g., Yoshida, 1959; O'Brien and Hurlburt, 1974; Cane, 1980; Reverdin and Cane, 1984; Reverdin, 1987; Han et al., 1999, 2001, 2004, 2011; Nagura and McPhaden, 2010a, b; Nyadjro and McPhaden, 2014), have greatly advanced our understanding for the general features and relevant mechanisms of WJs. Due to the variability of zonal wind forcing over TIO, equatorial surface WJs perform complex activities ranging from intraseasonal to decadal time scales (e.g., Reppin et al., 1999; Vinayachandran et al., 1999, 2007; Grodsky et al., 2001; Manghnani et al., 2003; Senan et al., 2003; Sengupta et al., 2001; Nagura and McPhaden, 2008, 2010a, b; Qiu et al., 2009; Chu, 2010; Gnanaseelan et al., 2012; Joseph et al., 2012; McPhaden et al., 2015; Duan et al., 2016; Sachidanandan et al., 2017; Wu et al., 2018). In addition, the equatorial wave dynamics have also well reproduced the seasonal circulation sys-

Foundation item: The Basic Scientific Fund for National Public Research Institutes of China under contract Nos 2019Q03 and 2017S02; the National Natural Science Foundation of China under contract Nos 41706032, 41406012, 4187060841, 41876028 and 41676020; Taishan Scholars Programs of Shandong Province under contract No. tsqn201909165; the National Program on Global Change and Air-Sea Interaction under contract Nos GASI-IPOVAI-03, GASI-IPOVAI-02, GASI-02-IND-STSaut and GASI-02-IND-STSwin; the NSFC-Shandong Joint Fund for Marine Science Research Centers under contract No. U1606405; the Ao-Shan Talents Cultivation Program supported by Pilot National Laboratory for Marine Science and Technology (Qingdao) under contract No. 2017ASTCP-OS01.
*Corresponding author, E-mail: liul@fio.org.cn

tem in the TIO (Jensen, 1993; Han et al., 1999, 2011; Yuan and Han, 2006; Nagura and McPhaden, 2010a; Chen et al., 2015a, b; Huang et al., 2018a, b). In particular, the semiannual WJs' dynamics controlled by the equatorial waves has been widely described, and it is found that the WJ variations are mainly controlled by the wind-forced Kelvin/Rossby wave and boundary-generated Rossby wave (Cane, 1980; Luyten and Roemmich, 1982; McPhaden, 1982; Han et al., 1999, 2001; Iskandar and McPhaden, 2011; Nagura and McPhaden, 2010a, b, 2012, 2016; Iskandar et al., 2016; Chen et al., 2017).

The recently international community made great effort to make up the observation over the TIO with the joint works from global countries and scientists during last two decades. As the successful implementation of Research Moored Array for African-Asian-Australian Monsoon Analysis and Prediction (RAMA; McPhaden et al., 2009) and Cooperative Indian Ocean Experiment on Intraseasonal Variability (CINDY)/Dynamics of the Madden-Julian Oscillation (DYNAMO) international field campaign (Zhang and Yoneyama, 2017), kinds of *in-situ* observations collected by numerous instrument, which provided higher spatial and temporal resolution as well as long term monitoring, encourage international community to investigate multi-scale variability of the WJs and the associated air-sea interactions (e.g., Masumoto et al., 2005; Iskandar and McPhaden, 2011; Nagura and McPhaden, 2012; McPhaden and Foltz, 2013; Moum et al., 2014, 2016; Jensen et al., 2015; Rao et al., 2016; Shinoda et al., 2013a, b, 2017). In particular, taking advantage of the long zonal velocity time series records from equatorial RAMA Acoustic Doppler Current Profilers (ADCPs) at 80.5°E and 90°E, Iskandar and McPhaden (2011) have shown that the near-surface layer responds directly to intraseasonal zonal wind stress forcing and subsequently propagates eastward in the form of oceanic Kelvin waves. Using an 8-year record from the same ADCP at 90°E, Rao et al. (2016) have provided a comprehensive description of the observed zonal flow and reviewed the governing mechanisms. In our previous paper, based on the ADCP observation at 85°E and numerical experiments, we have briefly reported that the anomalous WJs activities in 2013 primary result from the equatorial zonal wind anomalies associated with the strong intraseasonal oscillation events (Duan et al., 2016). However, all of their works mainly focused on the intraseasonal variability and the buildup process of the WJs, and detailed WJ evolution and the direct *in-situ* observation evidence of modulation of equatorial waves on the WJ was still insufficiency. Therefore, in this paper, we examine the detailed buildup and termination of the spring WJ in 2013 with two sub-surface Acoustic Doppler Current Profilers (ADCP) moorings in the eastern equatorial Indian Ocean (EqIO), and reveal the strong modulation of the equatorial waves on the WJ evolution.

2 Data and methods

2.1 *Data*

The analysis in the present study mainly utilizes daily average zonal velocity data from a RAMA upward-looking ADCP mooring at 0°, 80.5°E and a equatorial ADCP mooring deployed by the First Institute of Oceanography at 85°E. The 80.5°E data are available in 5 m vertical resolution from the surface down to 200 m depth, while the 85°E data are available in 10 m vertical resolution from April 5, 2013 to April 18, 2014 (Duan et al., 2016). Data shallower than about 30 m are discarded as they are contaminated by acoustic signals reflected off the surface. It is well worth to point out that we don't utilize the RAMA ADCP data at 0°, 90°E, which clearly displays an inconsequent WJ patterns, and the explanations are given in the Section 3.1.

Daily ocean temperature profiles at 80.5°E and 90°E are taken to describe the thermocline depth variability along the equator. And the Cross-Calibrated Multi-Platform (CCMP) V2.0 Level-3.5 (L3.5) gridded surface winds (Atlas et al., 2011) with a (1/4°) × (1/4°) spatial resolution was used to reveal the governing mechanism of the surface zonal jet.

The daily gridded sea level anomaly (SLA) data obtained from French Archiving, Validation, and Interpretation of Satellite Oceanographic data (AVISO) data center was applied to analysis the modulation of the equatorial waves on the WJ evolution. This reference delayed-time product, available with a (1/4°) × (1/4°) spatial resolution, merged data from ERS-1/2, TOPEX/Poseidon, Jason, and Envisat altimeters (Ducet et al., 2000). And Ocean Surface Current Analysis Real-time (OSCAR) provides the near-surface ocean current at a 15 m depth, combining geostrophic, Ekman and Stommel shear dynamics, and a complementary term from the surface buoyancy gradient (Bonjean and Lagerloef, 2002). The data is available as 5-day averages on a global (1/3°) × (1/3°) grid.

2.2 *Methods*

In order to reveal the dominated roles of equatorial wave dynamics in the WJ, the sea level decomposition method, following Boulanger and Menkes (1995), is adopted to separate the meridional modes of lone equatorial waves as follows:

$$h(x,y,t)=\sum_{0}^{n} r_n(x,t)\,R_n(y)\,, \tag{1}$$

$$r_n=\int_{-L}^{+L}\left(uR_n^u+hR_n^h\right)\mathrm{d}y, \tag{2}$$

$$L=(c/\beta)^{1/2}, \tag{3}$$

where r_n are the wave coefficients calculated by the method and R_n are longwave sea level structures (n=0 refers to Kelvin wave, $n\geqslant 1$ refers to the corresponding long Rossby wave mode; see also Figs 3a, b). The nondimensionalized zonal current u and SLA h are scaled with c and c^2/g respectively, where c=2 m/s is the baroclinic mode phase speed and g=9.81 m/s^2. For the calculation, the OSCAR data are first interpolated on to a daily regular grid as same as that of SLA data. See the detailed assumptions and projections method in the appendix of Boulanger and Menkes (1995). Following previous studies (Le Blanc and Boulanger, 2001; Nagura and McPhaden, 2010a, b, 2012, 2016; Iskandar and McPhaden, 2011), only the Kelvin wave and first meridional baroclinic Rossby wave were considered in the following context and high rank baroclinic wave modes were ignored.

3 Results

3.1 *Observed spring WJ onset and termination*

Figure 1 displays the evolution of the OLR, rainfall and surface zonal winds near the equator (5°N–5°S). The active atmospheric convection associated with a robust Madden-Julian Oscillation (MJO; Madden and Julian, 1971, 1972) was found in the TIO, initiating at the end of April and then propagating eastward along the equator. In association with the active convection phase, a pronounced westerly wind burst (WWB) presented in

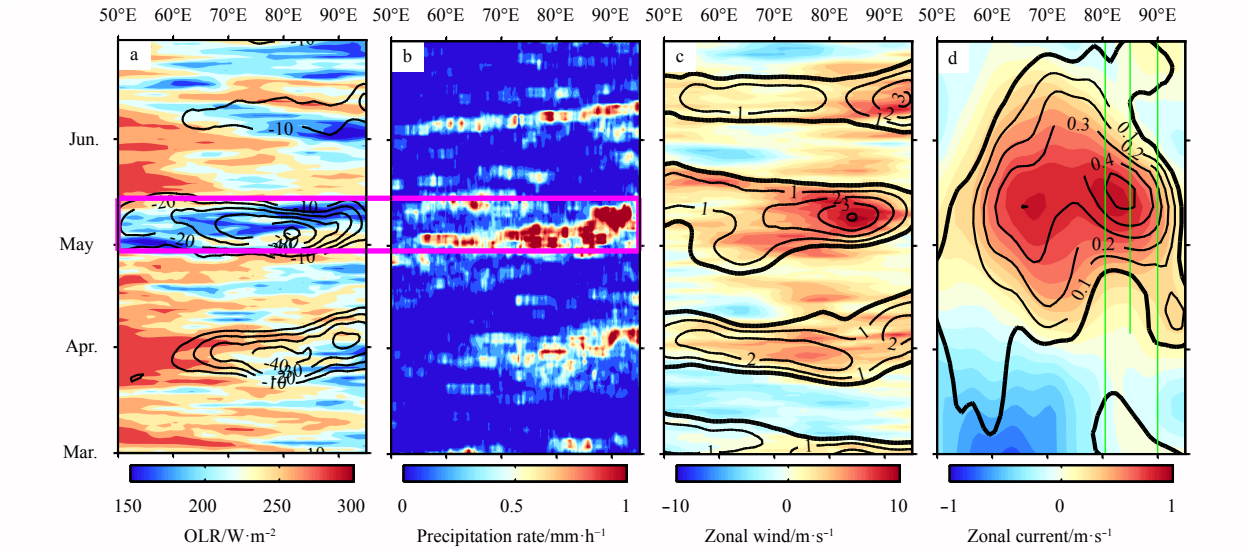

Fig. 1. Longitude-time diagrams of outgoing longwave radiation (a, OLR, W/m^2) from NOAA's Climate Data Record, TRMM precipitation rates (b, mm/h), CCMP zonal wind (c, m/s) averaged over 5°N–5°S and OSCAR zonal current (d, m/s) along the equator. The contours in Figs a and Figs c indicate their respective intraseasonal anomalies, and the magenta box in Figs a and b indicates the active phase of the MJO. The contours in Fig. d are the zonal current anomalies, and the green lines display the observation sites and available measurement.

the eastern basin at early May, and the strongest zonal winds exceeding 12 m/s were observed around 80°–90°E. From mid-May, atmospheric convection was largely suppressed, and corresponding surface zonal winds became much weaker.

Numerous studies have already demonstrated that WWB associated with the MJO event could produce strong equatorial jet within few days (Wyrtki, 1973; McPhaden, 1982; Schiller and Godfrey, 2003; Senan et al., 2003; Sengupta et al., 2007; Nagura and McPhaden, 2012; Shinoda et al., 2013a; Moum et al., 2014; Duan et al., 2016; Rao et al., 2016). Duan et al. (2016) pointed out

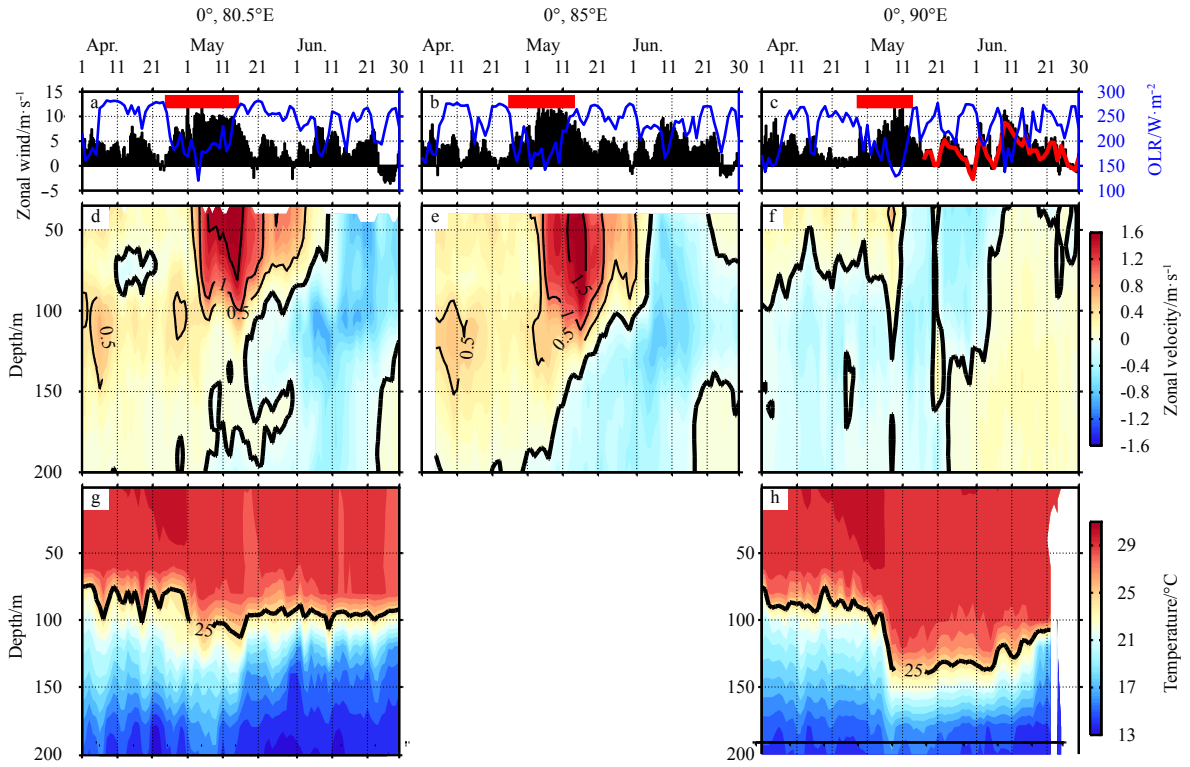

Fig. 2. Daily time series of CCMP zonal wind (black bars) and OLR (blue lines) (a–c), zonal velocity from ADCP moorings (d–f), upper ocean temperature at 0°, 80.5°E (left panel), 0°, 85°E (middle panel) and 0°, 90°E (right panel). Red horizontal lines in Figs a–c indicate the active phase of the MJO according to Fig. 1, and red thin line in Fig. c is the available zonal wind from the RAMA buoy.

that the spring WJ in 2013 was also largely modulated by WWB. Figure 2 illustrates the detailed evolution of surface zonal winds and the upper ocean current observed by two adjacent ADCP moorings in the eastern EqIO. Before the arrival of MJO-induced WWB, presence of an eastward flowing equatorial undercurrent (EUC) in the depth range of 80–150 m during April-early May is the dominant feature. And a very weak eastward surface current overlying the EUC was observed (Fig. 2d). Then an eastward jet at 80.5°E accelerated rapidly from < 0.5 m/s to 1.0 m/s within three days in early May. The main WJ structure (indicated by the threshold of 1.0 m/s for the zonal velocity) was located in the upper 110 m layer, with the zonal current speed in excess of 1.0 m/s between 5–22 May and a maximum of 1.76 m/s at May 14. The observed spring jet behaved just as a single intraseasonal event, consistent with the simulated results of Sengupta et al. (2007).

The evolution of spring WJ at 85°E presented similar features as that at 80.5°E (Fig. 2e, see also Table 1). The main jet structure was located in the upper 120 m layer, with a zonal velocity > 1.0 m/s between May 6–22 and a maximum of 1.83 m/s at May 16. Both dates of maximum zonal currents at 80.5°E and 85°E emerged near the end of the active phase of the MJO. Unlike the rapid accelerations, the zonal jet at 80.5°E and 85°E both experienced a subsequent slow weakening and shoaling process associated with the following relaxation of westerly wind forcing. The zonal current at 80.5°E reversed from eastward to westward at 10 June, while the jet termination at 85°E was 6 June, 4 days before the jet termination at 80.5°E. In addition, the WJ deceleration was clearly in advance of the reversal of the westerlies, indicating that the WJ termination may not be caused by surface wind forcing.

Table 1. The main characters of the observed spring WJ from ADCP moorings (zonal velocity u>1 m/s indicates the main WJ, while u<0 m/s means the WJ termination)

	u_{max} /m· s^{-1}	Date (u_{max})	Date range (u>1 m/s)	Date (u<0 m/s)
80.5°E	1.76	May 14	May 5–22	June 10
85°E	1.83	May 16	May 6–22	June 6

Moreover, in sharp contrast to that at 80.5°E and 85°E, there was no significant zonal jet at 90°E, although the overlying surface wind forcing is not weaker than the former sites at early May (Figs 2c and f). Only a much weaker eastward zonal current, with a peak zonal velocity of ~0.8 m/s at 8 May, was found in the upper 50 m layer. It should also be noted that the eastward current reverses its direction at 12 May, much earlier than those two western sites, although the local zonal winds were still eastward and greater than 7 m/s. However, all the outputs of the available open-accessed ocean reanalysis systems (e.g., HYCOM, SODA3, GODAS, ECMWF ORAS4, ECCO/ECCO2) and our simulated results (Duan et al., 2016) show a strong and long-lived zonal jet at 90°E (figures not shown). And the surface zonal current from OSCAR also indicated a zonal jet in the upper 30 m (Fig. 1d), which may be more consist with the current observations at 80.5°E and 85°E.

Another interesting phenomenon is the pronounced changes in the ocean thermocline. The temporal evolutions of upper-ocean temperature structure of the uppermost 200 m water column at 80.5°E and 90°E are also shown in Figs. 2g and h . During the suppressed MJO phase in mid-April, the thermocline, represented by the 25°C isotherm (D25), at 80.5°E was at the depth of about 80 m. Then it significantly deepened by about 30 m and lasted for about 17 d, which is produced by the strong zonal jet during the active MJO phase. And the upper layer temperature at 80.5°E decreased by almost 1.1°C (Fig. 2g), resulting from the combination of atmospheric cooling from above and enhanced vertical mixing from below (e.g., Schiller and Godfrey, 2003; Han et al., 2004; McPhaden and Foltz, 2013; Moum et al., 2014, 2016; Pujiana et al., 2018; Pujiana and McPhaden, 2018). The changes in the ocean thermocline at 90°E were ever more evident, deepening by almost 50 m at early May and persisting for more than one month (Fig. 2h). This great isopycnal movement also suggests that a strong zonal jet should present at 90°E. In addition, since the MJO-induced rainfall at 90°C is much stronger than 80.5°E and 85°E (Fig. 1b), the net fresh water flux could decrease the mixed layer by enhancing the near-surface stratification and then strengthen the surface WJ (Han et al., 1999; Masson et al., 2003). Furthermore, we have also examined the respective correlation between the zonal pressure gradient force (zonal gradient of SLA between three moorings and the eastern EqIO (1°S–1°N, 95°–100°E)) and the 80–140 m-averaged zonal current, and the current observations at 80.5°E and 85°E are quite consistent with previous studies (Chen et al., 2015a, 2019; Rao et al., 2016), but not that at 90°E. So, all these above results suggest that the ADCP data at 90°E may be incorrect and we thus neglect it in this paper.

3.2 *Role of equatorial waves on the WJ evolution*

As revealed by *in-situ* observations, since the spring WJ termination did not result from the surface wind forcing, the dynamical processes in the ocean interior may thus play the key role. Current observations (Figs 2d and e) illustrated there were significant baroclinic in the upper layer of the eastern EqIO. The lead-lag correlation coefficient of the zonal jets between 80.5°E and 85°E reaches 0.84 with an almost 3-day lag. Then the observed eastward phase propagation of the WJ was approximately 1.92 m/s, which is broadly commensurate with the phase speed of the baroclinic mode equatorial oceanic Kelvin waves (Le Blanc and Boulanger, 2001; Sengupta et al., 2007; Rao et al., 2016). In the surface layer, the buildup process of the eastward flowing WJ was accompanied with the downward isopycnal movements (Fig. 2g), showing the typical downwelling Kelvin wave responses (Webber et al., 2010; Iskandar and McPhaden, 2011; Moum et al., 2014; Rao et al., 2016). In the thermocline, the D25 signal at 80.5°E leading that at 90°E with a phase difference of about 6 days translates into propagation speed of about 2.02 m/s (Figs 2g and h), which also broadly agrees with the eastward propagation speed of the Kelvin wave along the equator.

Previous studies have reported that the zonal phase of seasonal WJ propagates mainly to the west in response to zonally propagating surface zonal winds (Molinari et al., 1990; Han et al., 1999; Qiu et al., 2009; Nagura and McPhaden, 2010a, b, 2016). However, the present moored records display that the spring WJ event in 2013 presented a distinct eastward-propagating pattern in the eastern EqIO, which results from the strong modulation of WWB-forced Kelvin wave. In order to further address the roles played by the wind-driven equatorial wave dynamics, the longitude-time diagram of SLA and corresponding decomposed Kelvin and Rossby waves modes are shown in Figs 3c and e. In response to the strong westerly winds occurring in late April (Fig. 1c), a prominent eastward propagation of the positive SLA is well captured in the eastern EqIO. The propagation speed is roughly 2.31 m/s, which is quite close to the phase speed of the Kelvin wave in this region (Nagura and McPhaden, 2010b; Iskandar et al., 2016). As the wind-forced equatorial Kelvin wave prevails over the eastern TIO, strong convergence by the zonal jet took

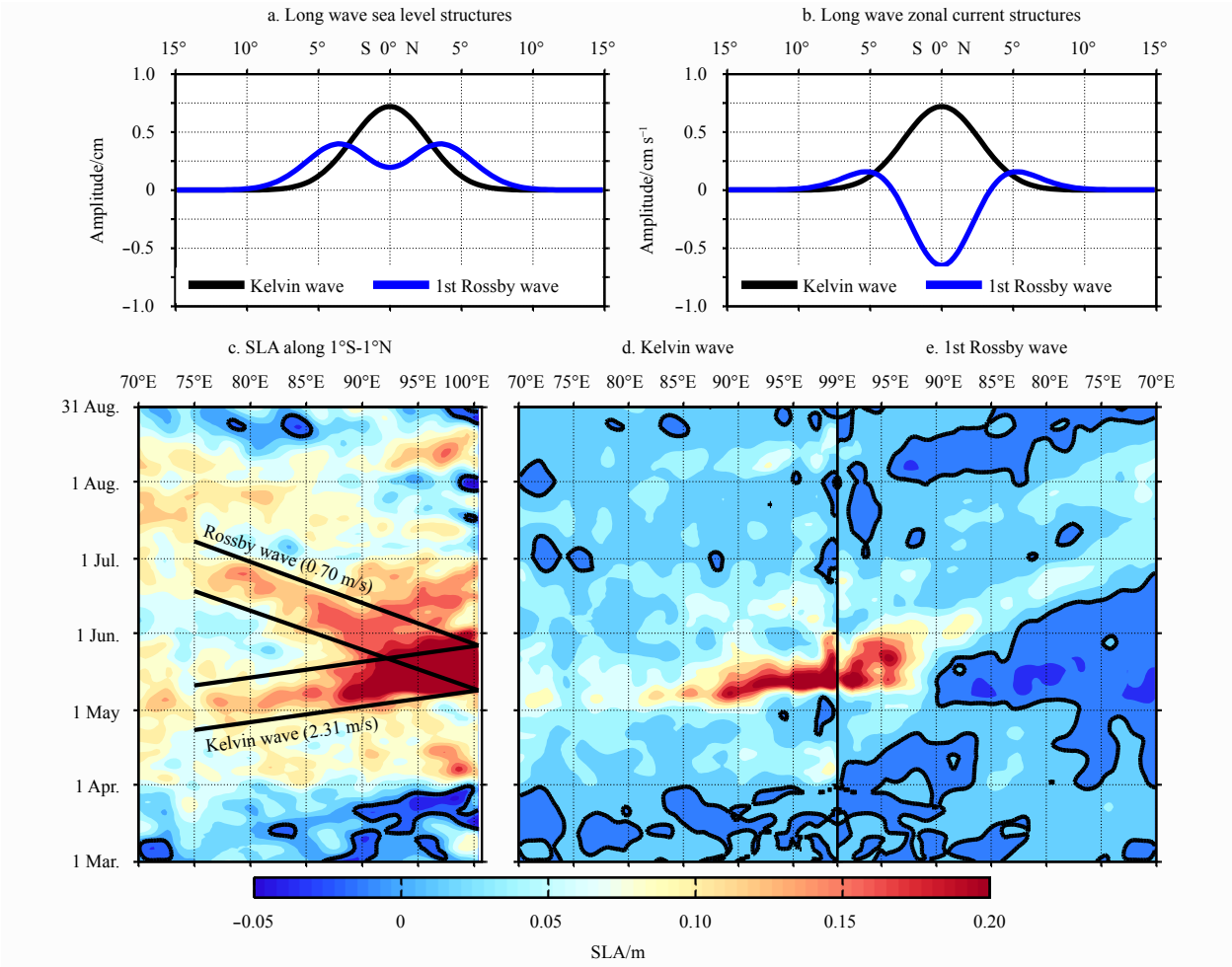

Fig. 3. Meridional structures of sea level (a) and zonal current (b) for Kelvin and first-Rossby modes (calculated for a 2 m/s Kelvin phase speed). Modified from Fig. 2 of Le Blanc and Boulanger (2001). Note that the Kelvin and first Rossby modes have the same sign in SLA but not in current. Longitude-time diagrams of SLA (c, cm), decomposed Kelvin wave (d, cm; from 70°E to 99°E) and Rossby wave (e, cm; in reverse display from 99°E to 70°E) along the equator averaged between 1°S and 1°N. The straight lines in Fig. c indicate the equatorial Kelvin and reflected Rossby wave beams. Contour interval in Figs c–e is 2 cm and the black contours indicate the zero lines.

place along the eastern boundary of the TIO, and then a significant SSH increase (~30 cm) was found along the coast of Sumatra in mid-May (Figs 3c and 4c).

By using a two-layer model, O'Brien and Hurlburt (1974) firstly noted that the reflected effect of eastern boundary of Indian Ocean was able to terminate WJ event. Analysis of altimeter data in 2013 had shown that the reflection of equatorial Kelvin wave into Rossby waves at the eastern boundary clearly. Figure 3c displays the westward propagation signal with speed 0.7 m/s, which matches well with the phase speed of the first baraclinic Rossby wave in this region (Le Blanc and Boulanger, 2001; Sengupta et al., 2007; Webber et al., 2012; Chen et al., 2017; Shinoda et al., 2017). Figure 3e further displays that projected first baraclinic Rossby wave westward propagation movement throughout the entire eastern basin from mid-May to late June, which is well consistent with the dates of the ocean zonal velocity reversal from eastward to westward observed by ADCP moorings (Figs 2d and e, Table 1).

A combination of the SLA and corresponding ocean surface current is also able to present more clearly the general diagram of how the equatorial waves modulating WJ termination in 2013. It displays that the rapid acceleration of eastward surface jet in early May was evident in almost the entire eastern basin, which is associated with the downwelling Kelvin wave propagates eastward from early- to mid-May (Figs 4a and c). And the large-scale eastward zonal currents became generally weaker from late May, when the westward propagating Rossby waves reflected from the Sumatra coast began to gradually decelerate the strong jet from east to west (Figs 4d and f). During mid- to late June, the westward-propagating Rossby wave can be further confirmed by the deepening of the thermocline from the RAMA moorings at 1.5°S, 80.5°E and 1.5°N, 80.5°E (figure not shown here).

4 Conclusions

Based on *in-situ* observations from two equatorial ADCP moorings at 80.5°E and 85°E, we have examined the entire evolution of spring WJ in 2013 and revealed the dominated governing role of equatorial waves on the WJ onset and termination in the present study. From late April to mid-May, a robust MJO propagates eastward across the TIO and causes a pronounced surface WWB in the eastern basin. The equatorial wave analysis demonstrated that the eastward-propagating Kelvin wave, induced by

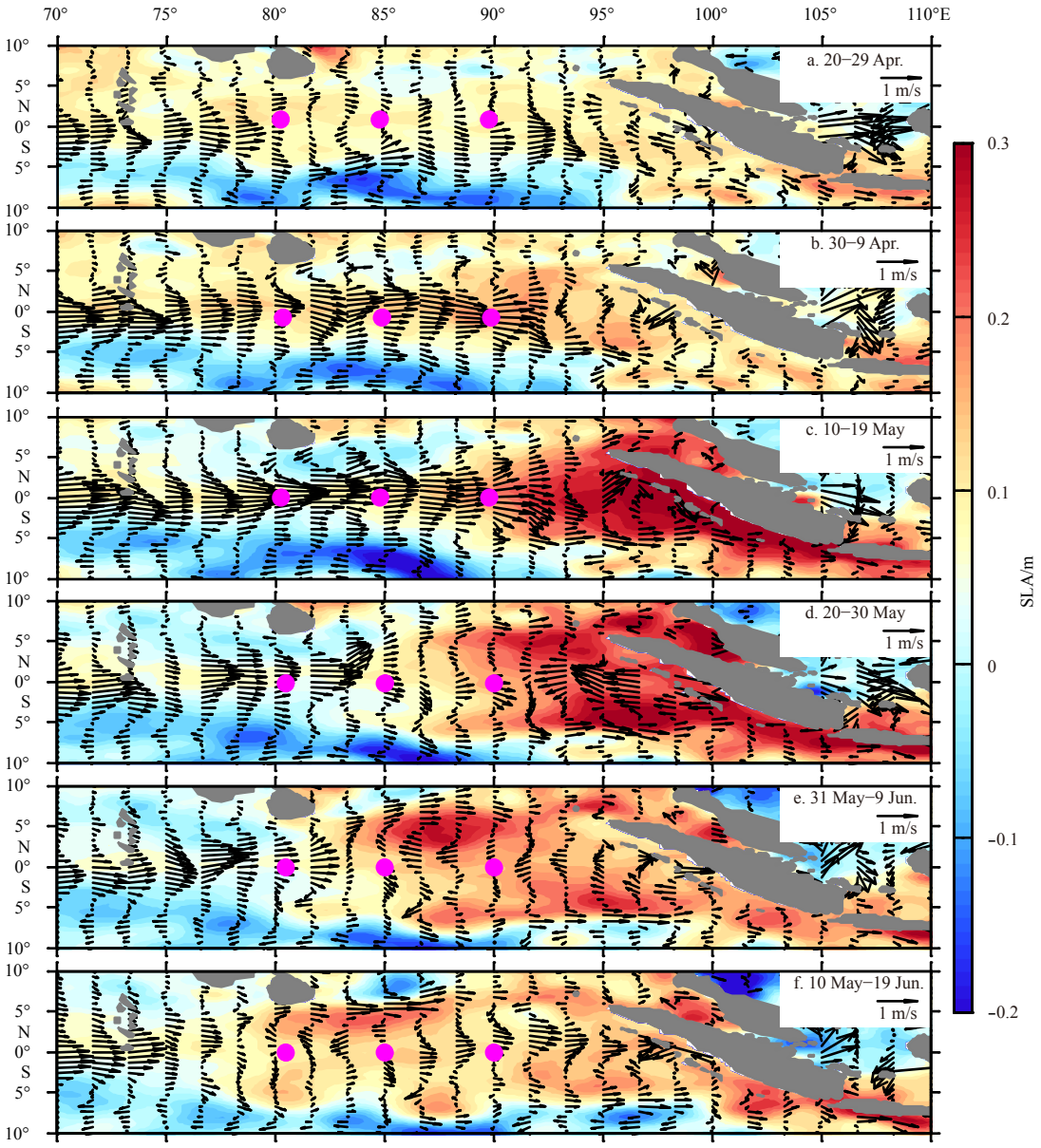

Fig. 4. Evolution of the averaged SLA (shading, m) from AVISO and corresponding urface currents (vector, m/s) from OSCAR. The mooring locations are marked by magenta dots.

the WWB, produced the strong equatorial jet in early May. The observed zonal jet presented thus as one intraseasonal event with a distinct eastward-propagating pattern in the eastern EqIO. In addition, the subsequent reflected Rossby waves radiating from eastern boundaries of the TIO not only modulated slightly the WJ strength/structure as proposed by previous studies but played a crucial role in the jet termination. The corresponding changes in the ocean thermocline also confirmed these strong modulations of equatorial waves on the WJ.

Acknowledgements

We sincerely appreciate the data freely used in this study, including the RAMA data obtained from https://www.pmel.noaa.gov/tao/drupal/disdel/, the altimeter data from http://www.aviso.altimetry.fr/en/data.html, the CCMP sea wind product from http://data.remss.com/, and the OSCAR data from http://apdrc.soest.hawaii.edu/data/. This work was also supported by Southern Marine Science and Engineering Guangdong Laboratory, Zhuhai.

References

Atlas R, Hoffman R N, Ardizzone J, et al. 2011. A cross-calibrated, multiplatform ocean surface wind velocity product for meteorological and oceanographic applications. Bulletin of the American Meteorological Society, 92(2): 157–174, doi: 10.1175/2010BAMS2946.1

Bonjean F, Lagerloef G S E. 2002. Diagnostic model and analysis of the surface currents in the tropical Pacific Ocean. Journal of Physical Oceanography, 32(10): 2938–2954, doi: 10.1175/1520-0485(2002)032<2938:DMAAOT>2.0.CO;2

Boulanger J P, Menkes C. 1995. Propagation and reflection of long equatorial waves in the Pacific Ocean during the 1992-1993 El Niño. Journal of Geophysical Research, 100(C12): 25041–25059, doi: 10.1029/95JC02956

Cane M A. 1980. On the dynamics of equatorial currents, with application to the Indian Ocean. Deep Sea Research Part A. Oceanographic Research Papers, 27(7): 525–544, doi: 10.1016/0198-

0149(80)90038-2
Chen Gengxin, Han Weiqing, Li Yuanlong, et al. 2015a. Seasonal-to-interannual time-scale dynamics of the equatorial undercurrent in the Indian Ocean. Journal of Physical Oceanography, 45(6): 1532–1553, doi: 10.1175/JPO-D-14-0225.1
Chen Gengxin, Han Weiqing, Li Yuanlong, et al. 2015b. Intraseasonal variability of upwelling in the equatorial eastern Indian Ocean. Journal of Geophysical Research, 120(11): 7598–7615
Chen Gengxin, Han Weiqing, Li Yuanlong, et al. 2017. Strong intraseasonal variability of meridional currents near 5°N in the eastern Indian Ocean: characteristics and causes. Journal of Physical Oceanography, 47(5): 979–998, doi: 10.1175/JPO-D-16-0250.1
Chen Gengxin, Han Weiqing, Li Yuanlong, et al. 2019. Intraseasonal variability of the Equatorial Undercurrent in the Indian Ocean. Journal of Physical Oceanography, 49(1): 85–101, doi: 10.1175/JPO-D-18-0151.1
Chu P C. 2010. Observational studies on association between eastward equatorial jet and Indian Ocean dipole. Journal of Oceanography, 66(3): 429–434, doi: 10.1007/s10872-010-0037-5
Duan Yongliang, Liu Lin, Han Guoqing, et al. 2016. Anomalous behaviors of Wyrtki jets in the equatorial Indian Ocean during 2013. Scientific Reports, 6(1): 29688, doi: 10.1038/srep29688
Ducet N, Le Traon P Y, Reverdin G. 2000. Global high-resolution mapping of ocean circulation from TOPEX/Poseidon and ERS-1 and -2. Journal of Geophysical Research, 105(C8): 19477–19498, doi: 10.1029/2000JC900063
Gnanaseelan C, Deshpande A, McPhaden M J. 2012. Impact of Indian Ocean Dipole and El Niño/Southern Oscillation wind-forcing on the Wyrtki jets. Journal of Geophysical Research, 117: C08005
Grodsky S A, Carton J A, Murtugudde R. 2001. Anomalous surface currents in the tropical Indian Ocean. Geophysical Research Letters, 28(22): 4207–4210, doi: 10.1029/2001GL013592
Han Weiqing, Lawrence D M, Webster P J. 2001. Dynamical response of equatorial Indian Ocean to intraseasonal winds: Zonal flow. Geophysical Research Letters, 28(22): 4215–4218, doi: 10.1029/2001GL013701
Han Weiqing, McCreary J P, Anderson D L T, et al. 1999. Dynamics of the eastern surface jets in the equatorial Indian Ocean. Journal of Physical Oceanography, 29(9): 2191–2209, doi: 10.1175/1520-0485(1999)029<2191:DOTESJ>2.0.CO;2
Han Weiqing, McCreary J P, Masumoto Y, et al. 2011. Basin resonances in the equatorial Indian Ocean. Journal of Physical Oceanography, 41(6): 1252–1270, doi: 10.1175/2011JPO4591.1
Han Weiqing, Webster P, Lukas R, et al. 2004. Impact of atmospheric intraseasonal variability in the Indian Ocean: Low-frequency rectification in equatorial surface current and transport. Journal of Physical Oceanography, 34(6): 1350–1372, doi: 10.1175/1520-0485(2004)034<1350:IOAIVI>2.0.CO;2
Huang Ke, McPhaden M J, Wang Dongxiao, et al. 2018a. Vertical propagation of middepth zonal currents associated with surface wind forcing in the equatorial Indian Ocean. Journal of Geophysical Research, 123(10): 7290–7307
Huang Ke, Wang Dongxiao, Wang Weiqiang, et al. 2018b. Multi-scale variability of the tropical Indian Ocean circulation system revealed by recent observations. Science China Earth Sciences, 61(6): 668–680, doi: 10.1007/s11430-017-9179-x
Iskandar I, McPhaden M J. 2011. Dynamics of wind-forced intraseasonal zonal current variations in the equatorial Indian Ocean. Journal of Geophysical Research, 116(C6): C06019
Iskandar I, Setiabudidaya D, Mardiansyah W, et al. 2016. Simulated interannual modulation of intraseasonal Kelvin waves in the equatorial Indian Ocean. Journal of Mathematical and Fundamental Sciences, 48(3): 213–229, doi: 10.5614/j.math.fund.sci.2016.48.3.3
Jensen T G. 1993. Equatorial variability and resonance in a wind-driven Indian Ocean model. Journal of Geophysical Research, 98(C12): 22533–22552, doi: 10.1029/93JC02565
Jensen T G, Shinoda T, Chen S, et al. 2015. Ocean Response to CINDY/DYNAMO MJOs in Air-Sea-Coupled COAMPS. Journal of the Meteorological Society of Japan, 93: 157–178
Joseph S, Wallcraft A J, Jensen T G, et al. 2012. Weakening of spring Wyrtki jets in the Indian Ocean during 2006–2011. Journal of Geophysical Research, 117: C04012
Le Blanc J L, Boulanger J P. 2001. Propagation and reflection of long equatorial waves in the Indian Ocean from TOPEX/Poseidon data during the 1993–1998 period. Climate Dynamics, 17(7): 547–557, doi: 10.1007/s003820000128
Liu Lin, Liu Baochao, Han Guoqing, et al. 2016. Assessment of the seasonal variation of simulated Wyrtki jet over the tropical Indian Ocean in CMIP5 models. Arabian Journal of Geosciences, 9: 676, doi: 10.1007/s12517-016-2704-3
Luyten J R, Roemmich D H. 1982. Equatorial currents at semi-annual period in the Indian Ocean. Journal of Physical Oceanography, 12(5): 406–413, doi: 10.1175/1520-0485(1982)012<0406:ECASAP>2.0.CO;2
Madden R A, Julian P R. 1971. Detection of a 40–50 day oscillation in the zonal wind in the tropical Pacific. Journal of the Atmospheric Sciences, 28(5): 702–708, doi: 10.1175/1520-0469(1971)028<0702:DOADOI>2.0.CO;2
Madden R A, Julian P R. 1972. Description of global-scale circulation cells in the tropics with a 40–50 day period. Journal of the Atmospheric Sciences, 29(6): 1109–1123, doi: 10.1175/1520-0469(1972)029<1109:DOGSCC>2.0.CO;2
Manghnani V, Subrahmanyam B, Xie Lian, et al. 2003. Numerical simulation of seasonal and interannual Indian Ocean upper layer circulation using Miami Isopycnic Coordinate Ocean Model. Journal of Geophysical Research, 108(C7): 3240, doi: 10.1029/2002JC001567
Masson S, Menkes C, Delecluse P, et al. 2003. Impacts of salinity on the eastern Indian Ocean during the termination of the fall Wyrtki Jet. Journal of Geophysical Research, 108(C3): 3067, doi: 10.1029/2001JC000833
Masumoto Y, Hase H, Kuroda Y, et al. 2005. Intraseasonal variability in the upper layer currents observed in the eastern equatorial Indian Ocean. Geophysical Research Letters, 32: L02607
McPhaden M J. 1982. Variability in the central equatorial Indian Ocean. Part I: Ocean dynamics. Journal of Marine Research, 40: 157–176
McPhaden M J, Foltz G R. 2013. Intraseasonal variations in the surface layer heat balance of the central equatorial Indian Ocean: The importance of zonal advection and vertical mixing. Geophysical Research Letters, 40(11): 2737–2741, doi: 10.1002/grl.50536
McPhaden M J, Meyers G, Ando K, et al. 2009. RAMA: The research moored array for African-Asian-Australian monsoon analysis and prediction. Bulletin of the American Meteorological Society, 90(4): 459–480, doi: 10.1175/2008BAMS2608.1
McPhaden M J, Wang Yi, Ravichandran M. 2015. Volume transports of the Wyrtki jets and their relationship to the Indian Ocean dipole. Journal of Geophysical Research, 120(8): 5302–5317
Molinari R L, Olson D, Reverdin G. 1990. Surface current distributions in the tropical Indian Ocean derived from compilations of surface buoy trajectories. Journal of Geophysical Research, 95(C5): 7217–7238, doi: 10.1029/JC095iC05p07217
Moum J N, De Szoeke S P, Smyth W D, et al. 2014. Air-sea interactions from westerly wind bursts during the November 2011 MJO in the Indian Ocean. Bulletin of the American Meteorological Society, 95(8): 1185–1199, doi: 10.1175/BAMS-D-12-00225.1
Moum J N, Pujiana K, Lien R C, et al. 2016. Ocean feedback to pulses of the Madden-Julian oscillation in the equatorial Indian Ocean. Nature Communications, 7(1): 13203, doi: 10.1038/ncomms13203
Nagura M, McPhaden M J. 2008. The dynamics of zonal current variations in the central equatorial Indian Ocean. Geophysical Research Letters, 35(23): L23603, doi: 10.1029/2008GL035961
Nagura M, McPhaden M J. 2010a. Wyrtki Jet dynamics: Seasonal variability. Journal of Geophysical Research, 115(C7): C07009
Nagura M, McPhaden M J. 2010b. Dynamics of zonal current variations associated with the Indian Ocean Dipole. Journal of Geo-

physical Research, 115(C11): C11026, doi: 10.1029/2010JC006423
Nagura M, McPhaden M J. 2012. The dynamics of wind-driven intraseasonal variability in the equatorial Indian Ocean. Journal of Geophysical Research, 117(C2): C02001
Nagura M, McPhaden M J. 2016. Zonal propagation of near-surface zonal currents in relation to surface wind forcing in the equatorial Indian Ocean. Journal of Physical Oceanography, 46(12): 3623–3638, doi: 10.1175/JPO-D-16-0157.1
Nyadjro E S, McPhaden M J. 2014. Variability of zonal currents in the eastern equatorial Indian Ocean on seasonal to interannual time scales. Journal of Geophysical Research, 119(11): 7969–7986
O'Brien J J, Hurlburt H E. 1974. Equatorial jet in the Indian Ocean: theory. Science, 184(4141): 1075–1077, doi: 10.1126/science.184.4141.1075
Pujiana K, McPhaden M J. 2018. Ocean surface layer response to convectively coupled kelvin waves in the eastern Equatorial Indian Ocean. Journal of Geophysical Research, 123(8): 5727–5741
Pujiana K, Moum J N, Smyth W D. 2018. The role of turbulence in redistributing upper-ocean heat, freshwater, and momentum in response to the MJO in the equatorial Indian Ocean. Journal of Physical Oceanography, 48(1): 197–220, doi: 10.1175/JPO-D-17-0146.1
Qiu Yun, Li Li, Yu Weidong. 2009. Behavior of the Wyrtki Jet observed with surface drifting buoys and satellite altimeter. Geophysical Research Letters, 36(18): L18607, doi: 10.1029/2009GL039120
Rao R R, Horii T, Masumoto Y, et al. 2016. Observed variability in the upper layers at the Equator, 90°E in the Indian Ocean during 2001–2008, 1: zonal currents. Climate Dynamics, 49(3): 1077–1105
Reppin J, Schott F A, Fischer J, et al. 1999. Equatorial currents and transports in the upper central Indian Ocean: Annual cycle and interannual variability. Journal of Geophysical Research, 104(C7): 15495–15514, doi: 10.1029/1999JC900093
Reverdin G. 1987. The upper equatorial Indian Ocean. The climatological seasonal cycle. Journal of Physical Oceanography, 17(7): 903–927, doi: 10.1175/1520-0485(1987)017<0903:TUEIOT>2.0.CO;2
Reverdin G, Cane M A. 1984. The near surface equatorial Indian Ocean in 1979. Part I: linear dynamics. Journal of Physical Oceanography, 14(12): 1817–1828
Sachidanandan C, Lengaigne M, Muraleedharan P M, et al. 2017. Interannual variability of zonal currents in the equatorial Indian Ocean: respective control of IOD and ENSO. Ocean Dynamics, 67(7): 857–873, doi: 10.1007/s10236-017-1061-4
Schiller A, Godfrey J S. 2003. Indian Ocean intraseasonal variability in an ocean general circulation model. Journal of Climate, 16(1): 21–39, doi: 10.1175/1520-0442(2003)016<0021:IOIVIA>2.0.CO;2
Schott F A, McCreary J P. 2001. The monsoon circulation of the Indian Ocean. Progress in Oceanography, 51(1): 1–123, doi: 10.1016/S0079-6611(01)00083-0
Schott F A, Xie Shangping, McCreary J P Jr. 2009. Indian Ocean circulation and climate variability. Reviews of Geophysics, 47(1): RG1002
Senan R, Sengupta D, Goswami B N. 2003. Intraseasonal "monsoon jets" in the equatorial Indian Ocean. Geophysical Research Letters, 30(14): 1750
Sengupta D, Goswami B N, Senan R. 2001. Coherent intraseasonal oscillations of ocean and atmosphere during the Asian Summer Monsoon. Geophysical Research Letters, 28(21): 4127–4130, doi: 10.1029/2001GL013587
Sengupta D, Senan R, Goswami B N, et al. 2007. Intraseasonal variability of equatorial Indian Ocean zonal currents. Journal of Climate, 20(13): 3036–3055, doi: 10.1175/JCLI4166.1
Shinoda T, Han Weiqing, Zamudio L, et al. 2017. Remote ocean response to the Madden-Julian Oscillation during the DYNAMO field campaign: Impact on Somali current system and the Seychelles-Chagos thermocline ridge. Atmosphere, 8(12): 171, doi: 10.3390/atmos8090171
Shinoda T, Jensen T G, Flatau M, et al. 2013a. Surface wind and upper-ocean variability associated with the Madden-Julian Oscillation simulated by the Coupled Ocean-Atmosphere Mesoscale Prediction System (COAMPS). Monthly Weather Review, 141(7): 2290–2307, doi: 10.1175/MWR-D-12-00273.1
Shinoda T, Jensen T G, Flatau M, et al. 2013b. Large-scale oceanic variability associated with the Madden-Julian Oscillation during the CINDY/DYNAMO field campaign from satellite observations. Remote Sensing, 5(5): 2072–2092, doi: 10.3390/rs5052072
Vinayachandran P N, Kurian J, Neema C P. 2007. Indian Ocean response to anomalous conditions in 2006. Geophysical Research Letters, 34(15): L15602
Vinayachandran P N, Saji N H, Yamagata T. 1999. Response of the equatorial Indian Ocean to an unusual wind event during 1994. Geophysical Research Letters, 26(11): 1613–1616, doi: 10.1029/1999GL900179
Webber B G M, Matthews A J, Heywood K J. 2010. A dynamical ocean feedback mechanism for the Madden-Julian oscillation. Quarterly Journal of the Royal Meteorological Society, 136(648): 740–754
Webber B G M, Matthews A J, Heywood K J, et al. 2012. Ocean Rossby waves as a triggering mechanism for primary Madden-Julian events. Quarterly Journal of the Royal Meteorological Society, 138(663): 514–527, doi: 10.1002/qj.936
Wu Yue, Liu Lin, Zhang Xinyou, et al. 2018. Different impacts from various El Niño events on Wyrtki jets in boreal autumn season. Pure and Applied Geophysics, 175(12): 4567–4577, doi: 10.1007/s00024-018-1928-4
Wyrtki K. 1973. An equatorial jet in the Indian Ocean. Science, 181(4096): 262–264, doi: 10.1126/science.181.4096.262
Yoshida K. 1959. A theory of the Cromwell Current and equatorial upwelling. Journal of the Oceanographical Society of Japan, 15: 154–170
Yuan Dongliang, Han Weiqing. 2006. Roles of equatorial waves and western boundary reflection in the seasonal circulation of the equatorial Indian Ocean. Journal of Physical Oceanography, 36(5): 930–944, doi: 10.1175/JPO2905.1
Zhang Chidong, Yoneyama K. 2017. CINDY/DYNAMO field campaign: Advancing our understanding of MJO initiation. In: World Scientific Series on Asia-Pacific Weather and Climate. Hackensack: World Scientific Publishing Co Pte Ltd, 339–348